Below Room Temperature C-H Bond Breaking on an Inexpensive Metal Oxide: Methanol to Formaldehyde on $CeO_2(111)$

Jonathan E. Sutton,[1]* Thomas Danielson,[2] Ariana Beste,[3] Aditya Savara[1]**

[1]*Chemical Sciences Division, Oak Ridge National Laboratory, Oak Ridge, TN, USA,*
[2]*Department of Materials Science and Engineering, Virginia Polytechnic Institute and State University, Blacksburg, VA, USA, (Present Address: Savannah River National Laboratory, Augusta, GA, USA)*
[3]*Joint Institute for Computational Sciences, University of Tennessee, Knoxville, TN. (Present Address: Army Research Laboratory, Adelphi, MD, USA)*

Author Contact Information: *suttonje@ornl.gov, **savaraa@ornl.gov

Abstract

Upgrading of primary alcohols by C-H bond breaking currently requires temperatures of > 200 °C. In this work, new understanding from simulation of a temperature programmed reaction study with methanol over a CeO_2(111) surface show C-H bond breaking -- and the subsequent desorption of formaldehyde -- even below room temperature. This is of particular interest because CeO_2 is a naturally abundant and inexpensive metal oxide. We combine density functional theory and kinetic Monte Carlo methods to show that the low temperature C-H bond breaking occurs via disproportionation of adjacent methoxy species. We further show from calculations that the same transition state with comparable activation energy exists for other primary alcohols; with ethanol, 1-propanol, and 1-butanol explicitly calculated. These findings indicate a promising class of transition states to search for in seeking low temperature C-H bond breaking over inexpensive oxides.

TOC Graphic

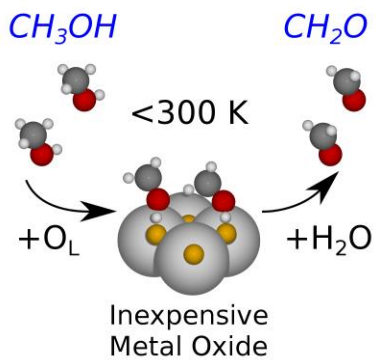

Conversion of renewable small organic oxygenates is of interest, including bio-ethanol and bio-butanol.(1-3) C-H bond breaking with release of the desired product is notoriously difficult to achieve at low temperatures, even for alcohols, with most catalytic examples comprising precious transition metals.(4-6) For example, one recent work showed methane C-H bond breaking at low temperature over Ir oxide,(7) but the surface intermediate remained without release until decomposition at >450 K. Relative to transition metals, non-transition metal processes tend to require even higher temperatures. The Formox process for converting methanol to formaldehyde on iron molybdates typically operates at temperatures above 300 °C.(8) Finding ways to (and understanding how to) accomplish C-H bond breaking at/below room temperature over cheap and abundant catalysts can open new areas of chemical reactions. In this letter, an exciting result is presented: formaldehyde can be produced by reaction of methanol over a CeO_2(111) surface, with the C-H bond breaking and formaldehyde release occurring even below room temperature. The solid catalyst, CeO_2, is cheap and naturally abundant. Additionally, the (111) crystal face is the most stable face. This work thus shows that methanol conversion to formaldehyde can occur on a cheap and abundant metal oxide at temperatures much lower than the previously reported value of 370K (which occurred in the presence of VOx/CeO_2(111)).(9)

Our approach involved using density functional theory (DFT) calculations to investigate the mechanism, and running Kinetic Monte Carlo simulations (KMC) for comparison with temperature programmed reaction (TPR) experimental data. For this work, TPR indicates that the solid catalyst was exposed to the reactant at temperatures below that of reaction, and that the temperature was then raised at a controlled and constant rate. It was found that below room temperature formaldehyde production over CeO_2(111) occurred by a disproportionation mechanism between neighboring methoxies. The Bell-Evans-Polanyi (BEP) principle was shown to exist for the activation energy of this reaction, and this correlation was found to extend beyond methanol: shown explicitly for ethanol, 1-propanol, and 1-butanol. These findings indicate that low temperature C-H bond breaking is possible over cheap metal oxides with release of the product molecule, when this type of transition state is accessible, and indicates that novel chemical processes may be discovered by searching for such reactions.

The experimental data was obtained by methanol exposure onto CeO_2(111) under ultrahigh vacuum at a temperature range where a monolayer would form (without multilayer formation), and then the sample was heated from 190 K to 800 K with a heating ramp of 2K/s (see reference and Supporting Information for details).(10) Correspondingly, the TPR simulations began with a full monolayer of methanol at 190 K (800 methanol molecules, on 800 Ce sites and 800 O sites). During simulation, the temperature was ramped at a rate of 2 K/s. As the temperature was ramped, various reactions and desorptions were observed in simulations, in accordance with experiment. The experimental data used was from reference (10). The CeO_2(111) was a thin film was grown on Ru(0001), as described previously.(11-12) The effects of co-adsorbates ("coverage effects") were included in the simulations. Further details of the DFT calculations, configurations, KMC methods,(13-14) several snapshots of the global surface configurations observed, and a table of the reactions and configurations that were used during simulations are provided in the Supporting Information. The supporting information also includes comparisons to experimental literature(15-16) for the simulated carbon containing species coverages as well as for the simulated Ce^{3+} ratio. The results of the simulated TPR signals are shown alongside the

experimental TPR data in Figure 1. Shaded boxes are shown as visual guides to the eye, and individual reactions are discussed in the text. In first principles simulation of TPRs involving more than simply desorption, perfect agreement is not expected.(17) Deviations are expected due to the errors associated with the energetics that come from DFT (estimated to be around 5-10 kcal/mol)(18), the use of assumed or estimated pre-exponentials in the rate constants of the simulations, as well as experimental sources of error. Given these sources of error, the agreement can be considered good when the simulation is within 50-100 K of the experimental peak and the peak areas are similar.(19)

In both experiment and simulation (Figure 1), the first observation is molecular desorption of methanol below 200 K, followed by water desorption at 225 K. From isotopically-labeled experiments, it is known that the desorbing water incorporates lattice O.(11) Subsequent to the initial water desorption, formaldehyde starts to desorb. In the experimentally obtained spectrum, the below room temperature formaldehyde peak is broad. The simulations show this peak more distinctly with essentially the same temperature range and peak area. This low temperature formaldehyde peak arising from methanol TPR over CeO_2(111) is also visible in previous work by another group, but was apparently not investigated further, at that time.(9, 20) In aggregate, there is sufficient agreement between theory and experiment for the areas and peak temperatures of methanol and formaldehyde desorption at below room temperature. In addition to the aforementioned sources of error, the differences may be due to imperfect capture of adsorbate-adsorbate repulsions as well as imperfect capture of the spatial distributions of species (including vacancies) at the surface. Both experiment and simulation then show a region without further peaks until $\geq$400 K, followed by a region where methanol and formaldehyde desorb at the same temperature. The concomitant desorption of methanol and formaldehyde above 400 K has resulted in conjecture that disproportionation produces that formaldehyde.(11, 15) We have found that disproportionation is also responsible for the below room temperature formaldehyde, and the differences between the two temperature ranges will be discussed.

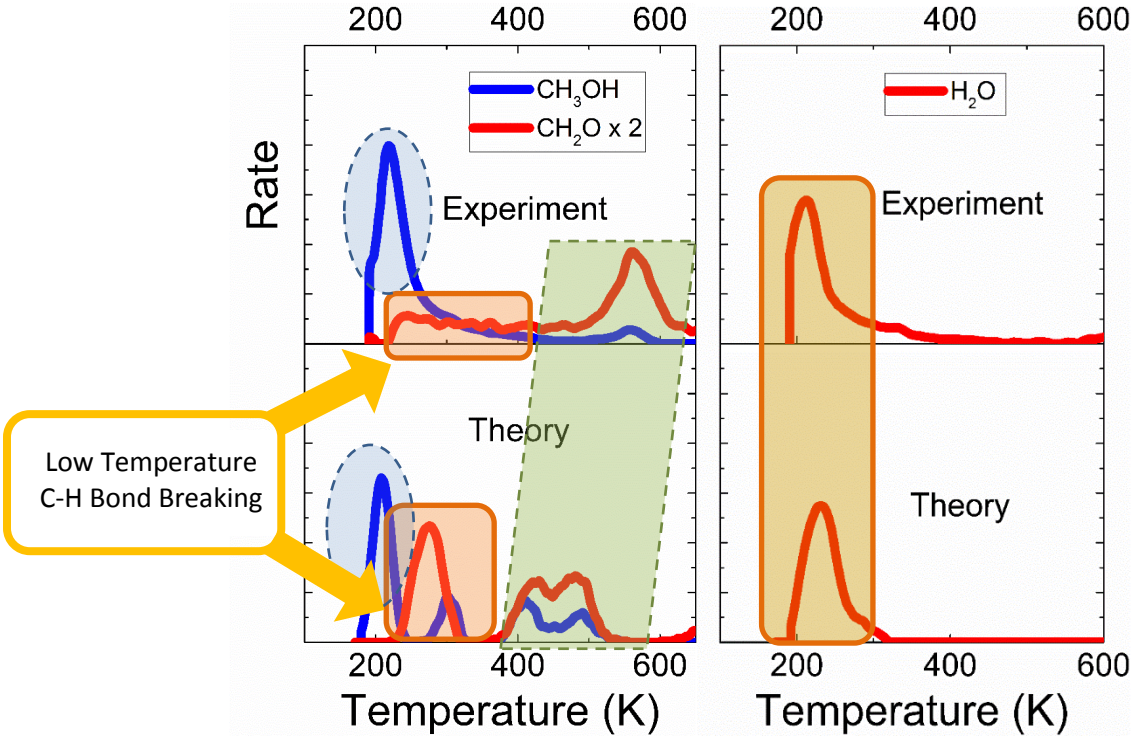

Figure 1. Comparison of experimental and theoretically simulated KMC spectra for the TPR after methanol adsorption on CeO_2(111). The shaded boxes are visual guides, the individual reactions are discussed in the text.

In interpreting the progression from the low temperature portion of the TPR experiment to the high temperature portion, we consider the elementary steps. The first step in the TPD mechanism is the molecular desorption of methanol (at <250 K). Once initial methanol desorption begins, water formation and subsequently water desorption occurs between 200-300 K. This water molecule formation occurs in a concerted step via participation of a lattice oxygen and two protons that originated from two different methanols.(21-22) After this concerted step, the water readily desorbs and a methoxy moves into the vacancy (making it short-lived), leaving one vacancy-methoxy and one atop-methoxy.(22) The rate of this water desorption is controlled by the rate of the concerted step (see Fig. S1 and S3 in the Supporting Information).

After water desorption, as the temperature increases, both gas-phase formaldehyde and gas-phase methanol are produced in processes that are kinetically limited by the rates of the surface reactions that make the molecules, as opposed to being desorption-limited. These molecular production processes occur in two temperature regions: below room temperature (<300 K) versus at elevated temperatures (>400K). There are thus at least two distinct reactions contributing to the gas-phase methanol and formaldehyde production peaks. In both temperature ranges, from the KMC simulations, it is possible to trace the gas-phase production peaks directly to originating from individual surface reactions from Table S1. We show the results of this tracing in Figure 2.

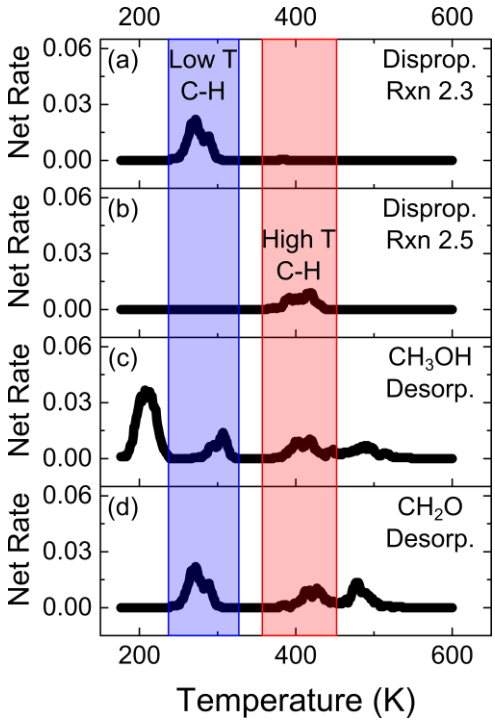

Figure 2. Simulated reaction rates for C-H bond breaking by disproportionation of adsorbed methoxy species reactions (Reactions 2.3 and 2.5, rates shown in panels a and b) and the total rates of formation of gas-phase methanol and formaldehyde (sum of rates of Reactions 5.3-5.8 shown in panel c and sum of rates of Reactions 7.1-7.4 shown in panel d). Colored panels indicate where the gas-phase methanol and formaldehyde formation occurs as a consequence of the relevant C-H bond breaking by disproportionation.

Figure 2 illustrates the contributions of the different elementary steps to the gas-phase peaks observed. The disproportionation between atop-methoxy species is Reaction 2.3 (rate shown in panel a), and results in the formation of gas-phase formaldehyde (275 K desorption peak in panel d) as well as the formation of gas-phase methanol (300 K desorption peak in panel c). In contrast, the disproportionation between an atop-methoxy and a vacancy-methoxy is Reaction 2.5 (rate shown in panel b), and results in nearly simultaneous formation of gas-phase formaldehyde and methanol (seen as 410 K desorption peaks in panels c and d). There are also peaks outside of the shaded regions: The methanol peak near 200 K is simply from methanol desorption, and the methanol and formaldehyde peaks above 450 K are due to direct C-H bond breaking (though the stoichiometry resembles disproportionation).

The relative positions of the sets of peaks in the shaded regions, associated with the two different types of disproportionation, are consistent with the energies of the associated transition state structures (shown in Figure 3) as well as the binding and activation energies (given in Table S1). In the case of the atop-atop disproportionation (Reaction 2.3), the transition state is very early (Figure 3a) with the C-H bond stretching just 0.04 Å. The activation barrier of 0.79 eV (Reaction 2.3, Table S1) is also quite accessible at 275 K. The formaldehyde formed from this process desorbs immediately, as the binding energy of formaldehyde near a methanol is 0.44 eV, which is lower than either the forward or reverse activation barriers for this disproportionation reaction. Methanol, on the other hand, has a binding-energy slightly higher than the activation energy of the low temperature disproportionation reaction

(0.84 eV when next to a formaldehyde; Reaction 5.5, Table S1) and therefore desorbs slightly later after the formaldehyde when the desorption energy is lower (0.81 eV; Reaction 5.8, Table S1).

Unlike the low temperature disproportionation process, the 410 K disproportionation process has the methanol desorbing slightly before the formaldehyde. This is consistent with the structure of the transition state (Figure 3b). Reaction 2.5 involves the transfer of an H from a vacancy-methoxy to an accepting atop-methoxy. Shortly after the H transfers, the methanol desorbs, leaving a formaldehyde in an O vacancy. This formaldehyde is more strongly bound (binding energy of 1.13 eV; Reaction 7.4, Table S1), and it desorbs slightly later after emerging from the vacancy.

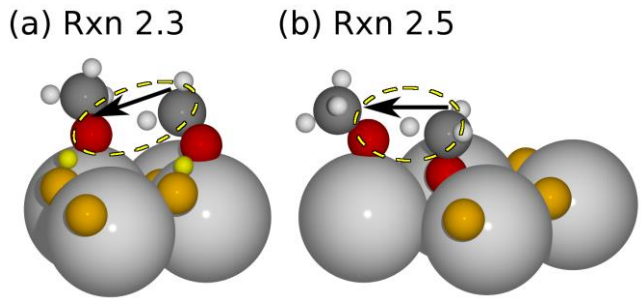

Figure 3. Images of methoxy disproportionation transition states for CeO_x(111), where the donating methoxy is either an atop-methoxy (Reaction 2.3, panel a) or a vacancy-methoxy (Reaction 2.5, panel b). Small white atoms are H, small yellow atoms are H adsorbed on surface O, medium gray atoms are C, medium red atoms are adsorbate O, medium orange atoms are surface O, and large gray atoms are Ce. H transfer paths are highlighted by dashed yellow ellipses. Black arrows indicate the direction of H transfer. Atomic radii are not to scale: For visual clarity, the radii depicted are based on covalent radii rather than crystal radii.

Though not the focus of this letter, at even higher temperatures, the production of methanol and formaldehyde are not correlated with a single irreversible process. Rather, there is a rapid cycle caused by Reactions 2.2, 2.5, 2.7, 9.2, and 9.3 (not plotted). The cycle was identified mechanistically by looking at the associated event frequencies in the simulations. This cycle begins with a vacancy-methoxy losing a H atom, primarily via simple dehydrogenation onto a surface O (Reaction 2.7) along with a competing contribution via disproportionation to make atop methanol (Reaction 2.5). In either case, the result is formaldehyde adsorbed in an O vacancy. This formaldehyde can move onto the surface (barrier of 0.23 eV; Reaction 9.2, Table S1). An atop-methoxy (possibly formed by atop formaldehyde scavenging a nearby H, via Reverse Reaction 2.2) can then jump into the vacancy (Reaction 9.3), closing the cycle.

Given that H_2O formation and desorption is facile, and also given that there is evidence of formaldehyde desorption from CeO_2 at ambient temperatures, we believe it should be possible to design a reactor and operating conditions under which the methanol to formaldehyde would be catalytic with H_2O as a co-product and an oxidant as an additional reactant (required to reoxidize the CeO_2 lattice). We have not attempted to find conditions to complete the catalytic cycle, though conducting such a future study is of interest. Some studies have suggested that cerium oxide may be able to adsorb and/or activate oxygen at or below room temperature(23-26), including in vacancies at CeO_2(111) surfaces(27). The activation may be modulated by crystal size for nanocrystals(28-29). Perhaps of even greater interest is the possibility of using CO_2 as the oxidant: a relatively recent study(30) has shown that CO_2 can reoxidize some vacancies after sufficient reduction of CeO_2(111).

Furthermore, this class of transition state should be more general than being confined to methanol. We speculated that this class of transition state should, at minimum, be generalizable to other primary alcohols. For example, the same transition state can be imagined for converting 1-butanol into butanal, which could provide a renewable route for plasticizer production. To test our belief that this class of transition state is more general than only for methanol, we performed a series of transition state searches for disproportionation involving other primary alkoxide species on Ce atop sites, in direct analogy to the low temperature elementary step found for methoxy disproportionation. We found the same class of transition states for all primary alkoxides ranging from one to four carbons (even longer chains were not tested, though we anticipate the same class of transition state to be applicable to longer chains). The resulting transition states are shown in Figure 4. All four transition states are extremely similar, with very slight increases in the length of the stretched C-H bond as a function of C number. We compiled the activation energies for the direct C-H and disproportionation reactions for methoxy in the presence of various co-adsorbates configurations and plotted these activation energies as a function of the reaction energy (along with the results for the disproportionation of the larger primary alcohols): BEP correlations were observed, as shown in Figure 5. The disproportionation reactions have a lower activation energy than direct C-H abstractions for any given reaction energy. The values associated with the primary alcohols are denoted by numbers and all fall on the same linear scaling relation associated with the various methoxy configurations, such that each of the primary alkoxy disproportionations display an activation energy below 1 eV.

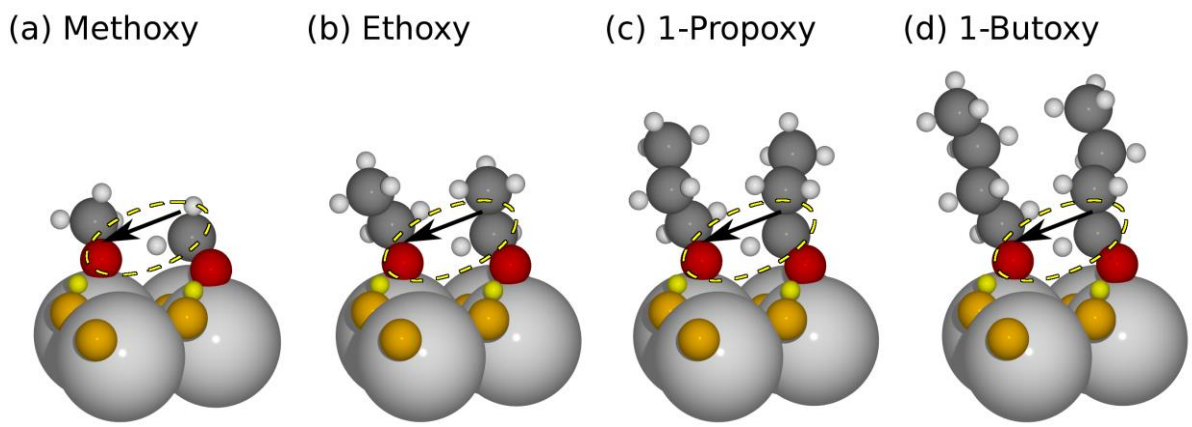

Figure 4. Images of (a) methoxy, (b) ethoxy, (c) 1-propoxy, and (d) 1-butoxy disproportionation transition states on pristine CeO_2(111). Small white atoms are H, small yellow atoms are H adsorbed on surface O, medium gray atoms are C, medium red atoms are adsorbate O, medium orange atoms are surface O, and large gray atoms are Ce. H transfer paths are highlighted by dashed yellow ellipses. Black arrows indicate the direction of H transfer. Atomic radii are not to scale: For visual clarity, the radii depicted are based on covalent radii rather than crystal radii.

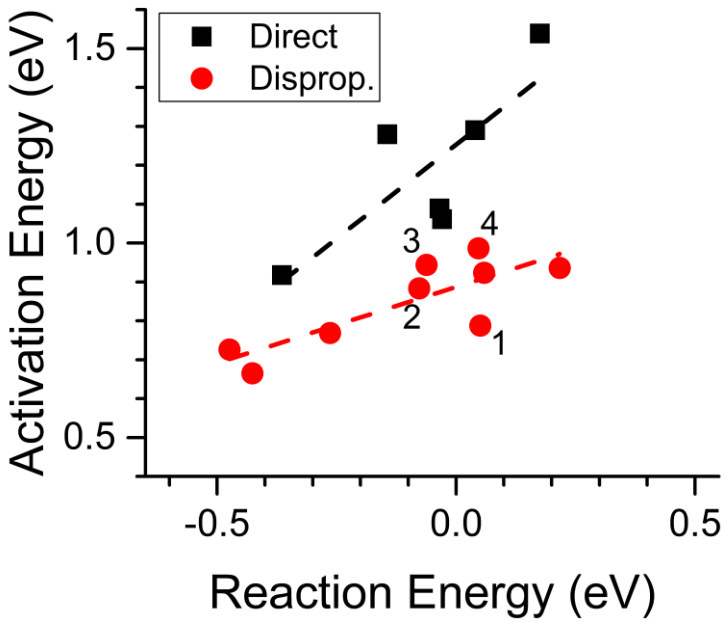

Figure 5. Activation energies E_A versus reaction energies ΔH for direct C-H scission and alkoxy disproportionation follow a BEP relation across a variety of adsorbate configurations. Disproportionation mechanisms are found to lower the activation energies. The trend is found to apply to not only methanol, but also to ethanol, 1-propanol, and 1-butanol, indicating generality. The disproportionation reactions between pairs of atop primary alkoxides are labeled as: 1 – methoxy, 2 – ethoxy, 3 – 1-propoxy, 4 – 1-butoxy. Dashed lines are from linear fits: for direct C-H cleavage, $\boldsymbol{E_A = 0.97\Delta H + 1.25}$; for disproportionation, $\boldsymbol{E_A = 0.39\Delta H + 0.89}$.

We have demonstrated that the most stable face of cerium oxide, an inexpensive metal oxide, can break the C-H bond in methanol below room temperature, with release of the molecular product of this C-H bond breaking to the gas-phase. The principal mechanism involved is a disproportionation between adjacent atop-methoxy species, Reaction 2.3: $2CH_3O@Ce_S \rightarrow CH_3OH@Ce_S + CH_2O@Ce_S$. We find that the same class of transition state exists for conversion of 1-butanol into butanal, and also for other primary alcohols. The class of transition states found indicates the importance of considering the potential energy surface for ensembles of adsorbates rather than simply individual reaction steps, as non-linear effects may be observed as a function of the number of adsorbates present (in this case, the effect is even similar but not identical to an autocatalytic effect – it is more similar to a chain-reaction propagation step). We believe it should be possible to design a reactor and operating conditions that enable the catalytic dehydrogenation of primary alcohols to the corresponding aldehydes, with a co-fed oxidant. This class of transition state can potentially open new chemistry and lead to new inexpensive metal oxide catalysts for conversion of renewable biomass feedstocks.

Acknowledgments

The major portion of this work (the DFT calculations and creation of the KMC model) was supported by the Laboratory Directed Research and Development Program of Oak Ridge National Laboratory, managed by UT-Battelle, LLC, for the U. S. Department of Energy. A minor portion of this work (running the KMC simulations for comparison with experiment) was supported by the U.S. Department of Energy,

Office of Science, Basic Energy Sciences, Chemical Sciences, Geosciences, and Biosciences Division. The authors thank D.R. Mullins for providing the experimental data. This research used resources of the Oak Ridge Leadership Computing Facility at the Oak Ridge National Laboratory, which is supported by the Office of Science of the U.S. Department of Energy under Contract No. DE-AC05-00OR22725.

Supporting Information available:

Additional details on the DFT Calculations, KMC methods, a table of the reactions and configurations that were used during simulations, a figure comparing the rates of water formation and desorption, adsorbate and surface cation concentrations as functions of temperature, global lattice configurations at select temperatures, and a discussion of the post-processing performed on the experimental data to generate the TPD spectra.

References

1. Taarning, E.; Osmundsen, C. M.; Yang, X.; Voss, B.; Andersen, S. I.; Christensen, C. H. Zeolite-Catalyzed Biomass Conversion to Fuels and Chemicals. *Energy Environ. Sci.* **2011**, *4*, 793-804.
2. Dahmen, M.; Marquardt, W. Model-Based Formulation of Biofuel Blends by Simultaneous Product and Pathway Design. *Energy Fuels* **2017**, *31*, 4096-4121.
3. Balat, M. Production of Bioethanol from Lignocellulosic Materials via the Biochemical Pathway: A Review. *Energy Convers. and Manage.* **2011**, *52*, 858-875.
4. Mallat, T.; Baiker, A. Oxidation of Alcohols with Molecular Oxygen on Solid Catalysts. *Chem. Rev.* **2004**, *104*, 3037-3058.
5. Wittstock, A.; Zielasek, V.; Biener, J.; Friend, C. M.; Bäumer, M. Nanoporous Gold Catalysts for Selective Gas-Phase Oxidative Coupling of Methanol at Low Temperature. *Science* **2010**, *327*, 319-322.
6. Deshlahra, P.; Iglesia, E. Reactivity and Selectivity Descriptors for the Activation of C–H Bonds in Hydrocarbons and Oxygenates on Metal Oxides. *J. Phys. Chem. C* **2016**, *120*, 16741-16760.
7. Liang, Z.; Li, T.; Kim, M.; Asthagiri, A.; Weaver, J. F. Low-Temperature Activation of Methane on the IrO_2(110) Surface. *Science* **2017**, *356*, 299-303.
8. Bahmanpour, A. M.; Hoadley, A.; Tanksale, A. Critical Review and Exergy Analysis of Formaldehyde Production Processes. *Rev. Chem. Eng.* **2014**, *30*, 583-604.
9. Ganduglia-Pirovano, M. V.; Popa, C.; Sauer, J.; Abbott, H.; Uhl, A.; Baron, M.; Stacchiola, D.; Bondarchuk, O.; Shaikhutdinov, S.; Freund, H.-J. Role of Ceria in Oxidative Dehydrogenation on Supported Vanadia Catalysts. *J. Am. Chem. Soc.* **2010**, *132*, 2345-2349.
10. Mullins, D. R.; Albrecht, P. M.; Calaza, F. Variations in Reactivity on Different Crystallographic Orientations of Cerium Oxide. *Top. Catal.* **2013**, *56*, 1345-1362.
11. Mullins, D. R.; Robbins, M. D.; Zhou, J. Adsorption and Reaction of Methanol on Thin-Film Cerium Oxide. *Surf. Sci.* **2006**, *600*, 1547-1558.
12. Mullins, D. R.; Radulovic, P. V.; Overbury, S. H. Ordered Cerium Oxide Thin Films Grown on Ru(0001) and Ni(111). *Surf. Sci.* **1999**, *429*, 186-198.
13. Danielson, T.; Sutton, J. E.; Hin, C.; Savara, A. SQERTSS: Dynamic Rank Based Throttling of Transition Probabilities in Kinetic Monte Carlo Simulations. *Comput. Phys. Commun.* **2017**, *219*, 149-163.
14. Hoffmann, M. J.; Matera, S.; Reuter, K. kmos: A Lattice Kinetic Monte Carlo Framework. *Comput. Phys. Commun.* **2014**, *185*, 2138-2150.
15. Albrecht, P. M.; Mullins, D. R. Adsorption and Reaction of Methanol over CeOx(100) Thin Films. *Langmuir* **2013**, *29*, 4559-4567.

16. Matolin, V.; Libra, J.; Skoda, M.; Tsud, N.; Prince, K. C.; Skala, T. Methanol Adsorption on a CeO_2(111)/Cu(111) Thin Film Model Catalyst. *Surf. Sci.* **2009**, *603*, 1087-1092.
17. Savara, A. Simulation and Fitting of Complex Reaction Network TPR: The Key is the Objective Function. *Surf. Sci.* **2016**, *653*, 169-180.
18. Sutton, J. E.; Guo, W.; Katsoulakis, M. A.; Vlachos, D. G. Effects of Correlated Parameters and Uncertainty in Electronic-Structure-Based Chemical Kinetic Modelling. *Nat. Chem.* **2016**, *8*, 331-337.
19. Masel, R. I., *Principles of Adsorption and Reaction on Solid Surfaces*; Wiley, 1996.
20. Abbott, H. L.; Uhl, A.; Baron, M.; Lei, Y.; Meyer, R. J.; Stacchiola, D. J.; Bondarchuk, O.; Shaikhutdinov, S.; Freund, H. J. Relating Methanol Oxidation to the Structure of Ceria-Supported Vanadia Monolayer Catalysts. *J. Catal.* **2010**, *272*, 82-91.
21. Mullins, D. R.; Senanayake, S. D.; Chen, T. L. Adsorption and Reaction of C1−C3Alcohols over CeOX(111) Thin Films. *J. Phys. Chem. C* **2010**, *114*, 17112-17119.
22. Sutton, J. E.; Overbury, S. H.; Beste, A. Coadsorbed Species Explain the Mechanism of Methanol Temperature-Programmed Desorption on CeO_2(111). *J. Phys. Chem. C* **2016**, *120*, 7241-7247.
23. Mullins, D. R. The Surface Chemistry of Cerium Oxide. *Surf. Sci. Rep.* **2015**, *70*, 42-85.
24. Li, C.; Xin, Q.; Guo, X. X. Surface Oxygen Species and Their Reactivities in the Mild Oxidation of Ethylene on Cerium Oxide Studied by Ft-Ir Spectroscopy. *Catal. Lett.* **1992**, *12*, 297-306.
25. Guzman, J.; Carrettin, S.; Corma, A. Spectroscopic Evidence for the Supply of Reactive Oxygen during CO Oxidation Catalyzed by Gold Supported on Nanocrystalline CeO2. *J. Am. Chem. Soc.* **2005**, *127*, 3286-3287.
26. Wu, Z.; Li, M.; Howe, J.; Meyer, H. M.; Overbury, S. H. Probing Defect Sites on CeO_2 Nanocrystals with Well-Defined Surface Planes by Raman Spectroscopy and O2 Adsorption. *Langmuir* **2010**, *26*, 16595-16606.
27. Zhao, Y.; Teng, B.-T.; Wen, X.-D.; Zhao, Y.; Chen, Q.-P.; Zhao, L.-H.; Luo, M.-F. Superoxide and Peroxide Species on CeO_2(111), and Their Oxidation Roles. *J. Phys. Chem. C* **2012**, *116*, 15986-15991.
28. Migani, A.; Vayssilov, G. N.; Bromley, S. T.; Illas, F.; Neyman, K. M. Greatly facilitated oxygen vacancy formation in ceria nanocrystallites. *Chemical Communications* **2010**, *46*, 5936-5938.
29. Vayssilov, G. N.; Lykhach, Y.; Migani, A.; Staudt, T.; Petrova, G. P.; Tsud, N.; Skála, T.; Bruix, A.; Illas, F.; Prince, K. C., et al. Support Nanostructure Boosts Oxygen Transfer to Catalytically Active Platinum Nanoparticles. *Nat. Mater.* **2011**, *10*, 310-315.
30. Staudt, T.; Lykhach, Y.; Tsud, N.; Skála, T.; Prince, K. C.; Matolín, V.; Libuda, J. Ceria Reoxidation by CO_2: A Model Study. *J. Catal.* **2010**, *275*, 181-185.